PUBLICATIONS OF THE ASTRONOMICAL SOCIETY OF THE PACIFIC, **116**:734–744, 2004 August

Photometric and Astrometric Analysis of Gemini/Hokupa'a Galactic Center Adaptive Optics Observations

JULIAN C. CHRISTOU AND GIOVANNA PUGLIESE[1]

Center for Adaptive Optics, University of California, 1156 High Street, Santa Cruz, CA 95064

RAINER KÖHLER

Max-Planck-Institüt für Astronomie, Königstuhl 17, D-69117 Heidelberg, Germany

AND

JACK D. DRUMMOND

Starfire Optical Range, Directed Energy Directorate, Air Force Research Laboratory, Kirtland AFB, NM 87117-5776

Received 2004 March 18; accepted 2004 June 18; published 2004 July 29

ABSTRACT. We have compared three techniques—StarFinder, IDAC (Iterative Deconvolution Algorithm in C), and parametric blind deconvolution (PBD)—for extracting photometry and astrometry of stars in densely crowded field adaptive optics observations, and their point-spread functions (PSFs). The three algorithms investigated produce very similar results over dynamic ranges of 4 mag, accurately measuring relative photometry to within 0.1 mag for dynamic ranges of 5 mag, as well as astrometry to within 10% of the PSF width. At larger dynamic ranges, the photometry is more dependent upon the field crowding, the signal-to-noise ratio, and the algorithm used.

1. INTRODUCTION

Adaptive optics (AO) for astronomy is now a mature field, with AO systems either currently installed or in preparation at the world's largest telescopes. These systems have been primarily, but not exclusively, used for imaging. However, the AO systems do not provide perfect correction, and there are residual wave-front errors that prevent the point-spread functions (PSFs) of the system from becoming fully diffraction-limited. The performance of an AO system is generally given by the Strehl ratio. This is the ratio of the peak of the AO PSF to that of a system's fully diffraction-limited PSF when both are normalized to the same volume. For most AO systems operating at near-infrared wavelengths, typical Strehl ratios are in the range of 20%–50%, and in poorer conditions or for fainter guide stars, usable AO images can be obtained with Strehl ratios of ~5%–10%. In addition, knowledge of the PSF during the observation is generally poor unless a relatively bright point source lies in the field. A point-source reference is needed for quantitative analysis and is generally obtained from observations of an unresolved source taken under conditions as similar as possible to the scientific target. This reference is generally observed in a separate field and at a different time, which leads to poor PSF calibration.

Over the past few years, a number of algorithms that extract estimates of the PSF from the observations themselves have been developed for application to AO data. These fall into the general category of "blind" deconvolution. Their application for the photometric and astrometric analysis of binary stars observed under less than optimal AO correction has been demonstrated (Barnaby et al. 2000). There are two types of blind deconvolution: the parametric approach (PBD), which models both the target and the PSF, and the iterative pixel-by-pixel reconstruction of each (IBD). The former measures the photometry and astrometry directly, and the latter requires the application of a photometry-measuring algorithm to the reconstructed target. A hybrid scheme has also been developed in which the PSFs are reconstructed on a pixel-by-pixel basis from the data, and the multiple point-source target is modeled by a set of δ-functions (Fusco et al. 1999). In addition, an algorithm for direct photometric and astrometric measurements from AO data has been developed for multiple point-source fields (StarFinder; Diolaiti et al. 2000) using a pixel-by-pixel PSF measured from the field.

In this paper we compare two generally available algorithms, IDAC and StarFinder, in addition to a PBD algorithm, for recovering quantitative science for AO observations obtained under poor compensation. These observations are of the Galactic center region, obtained during the commissioning of the Gemini North telescope using the 36 element Hokupa'a AO system (Graves et al. 2000). This system was initially developed for the Canada-France-Hawaii 3.6 m telescope (CFHT),

[1] Current address: European Southern Observatory, Garching-bie-München, Germany.

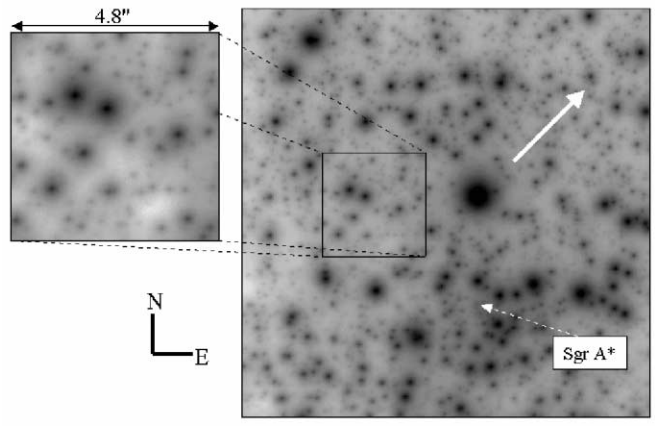

FIG. 1.—Gemini/Hokupa'a image of the Galactic center region in K'. Note the density of sources and the overlapping PSF structure. Also note the PSF variability (anioplanatism) across the field. The white arrow points to the $R = 13$ guide star approximately 30″ distant. The location of Sgr A* is also shown. The analysis was performed on the shown subfield, avoiding regions of saturation, anioplanatism, and extended sources. Images displayed on a logarithmic scale.

as opposed to an 8 m aperture, and so did not produce diffraction-limited images on this field, because of a relatively faint guide star ($R = 13$) that was 30″ from Sgr A*. In addition, the Galactic center cluster is extremely crowded, with many overlapping point sources in the field, especially with 0.″2 resolution, adding an extra order of complexity for the recovery of the photometry and astrometry.

An isoplanatic subfield in which the PSF is spatially invariant was chosen for the analysis. The iterative blind deconvolution algorithm IDAC (Christou et al. 1999), the PBD algorithm, and the photometry algorithm StarFinder were applied to the data, and the results demonstrate good agreement between the measurements. In order to determine the accuracy of the results, a set of data simulating the observations was generated. The simulation results showed that the astrometry from these techniques was equivalent to within ~10 mas, but that the StarFinder photometry was better. This is not surprising, since StarFinder is a target model fitting approach, whereas IDAC uses an aperture photometry package that is sensitive to nearby companions. Even so, these approaches demonstrated that for dynamic ranges of ~4–5 mag, the relative magnitude errors were small (~0.1 mag). Thus, both approaches are applicable to densely crowded fields for the extraction of photometric and astrometric information.

2. DATA

The Galactic center data set used for this analysis is part of the publicly available Gemini-North demonstration science data package GN-2000QS-DS-1, obtained in 2000 July and August[2]

[2] See http://www.us-gemini.noao.edu/gallery/science/gal_center.html.

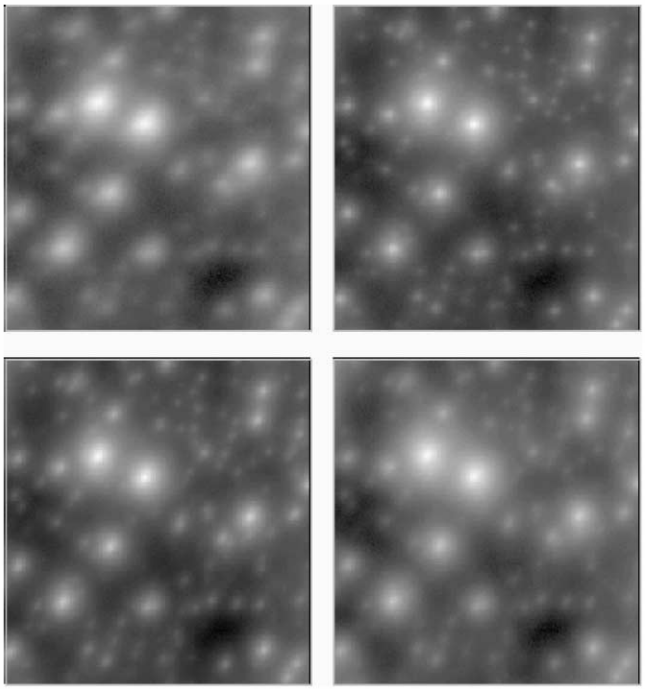

FIG. 2.—Isoplanatic 4.″8 × 4.″8 subfields of the four separate 30 s observations used for the analysis. Note the variable compensation for the observations. This is not surprising, since the four data sets were obtained on four different nights: *top left*: frame 1, 2000 July 2; *top right*: frame 2, 2000 July 3; *bottom left*: frame 3, 2000 July 4; and *bottom right*: frame 4, 2000 July 30. All images displayed on a logarithmic scale.

using the Hokupa'a AO system and QUIRC near-infrared imager. Hokupa'a is a 36 element curvature system that was originally designed for use with the 3.6 m CFHT. Gemini-North performance with this system typically provides on-axis Strehl ratios of ~5%–20% (Roth et al. 2001). QUIRC (the Quick Infrared Camera) is a 1024 × 1024 imager with an image scale of 18.9 mas pixel^{-1}, giving a 20″ × 20″ field size. The image scale means that the data were over–Nyquist-sampled, since the diffraction limit at the observing wavelength of 2.16 μm is 58.3 mas, corresponding to a critical sampling of 29.2 mas. The basic data processing for the Gemini-North demonstration data is described by Flicker & Rigaut (2002).

Figure 1 shows one of four 20″ × 20″ 30 s K' exposures of the Galactic center, known as field 1 in the demonstration science data. This image illustrates the density of the stars within this region, the overlapping PSFs, and the changing shape of the PSFs across the field. For the analysis presented here, we chose a smaller subfield of 4.″8 × 4.″8 (also shown) over which the PSF was spatially invariant, which is necessary for the application of StarFinder and IDAC. This region also avoided areas of saturation and extended sources, since the aim of the analysis was to investigate the ability to recover the relative astrometry and photometry. The corresponding four subfields are shown in Figure 2. The variability of the compensation

over the four exposures is clearly seen, as is the density of the stars within this relatively small field. Because of the poor compensation due to the faint, off-axis guide star, the full widths at half-maximum (FWHMs) for the four frames are ~0.″2; i.e., almost 4 times worse than diffraction-limited and Strehl ratios were estimated to be (~5%). A detailed study of the anisoplanatism in the demonstration science data set is given by Flicker & Rigaut (2002).

2.1. Algorithms

StarFinder solves for a numerical PSF on a pixel-by-pixel basis from the field and then fits this PSF to the locations of the maxima to obtain the relative photometry and astrometry of the stars. IDAC is a multiframe blind deconvolution (MFBD) algorithm that numerically solves for both the PSF and the target simultaneously. Photometry is then performed on the deconvolved target. PBD fits the PSF with an analytical form and uses this PSF to extract the relative photometry and astrometry. Thus, both StarFinder and PBD constrain the target to the specific model, unlike the iterative blind deconvolution approach. Also, both StarFinder and IDAC allow the PSF to take on any form determined from the data, whereas PBD constrains it to the model used. The StarFinder and IDAC codes are available form the Center for Adaptive Optics Web site.[3]

2.2. StarFinder

The StarFinder code, which runs under IDL, was developed for the specific purpose of measuring the relative photometry and astrometry from an AO-corrected field. However, in this case, the density of objects in the field is much higher than the test cases (Diolaiti et al. 2000). The algorithm is explained in detail elsewhere, and just an overview of how it works is presented here. In order to compute the relative photometry and astrometry in the data, the algorithm first has to solve for a PSF. This is done interactively by selecting brighter, more isolated stars out to a given radius, computing their centroids, and averaging these stars together. The effect of nearby companions is reduced by selecting their positions by eye, as well as limiting the extent of the PSF. Generating the PSF was found to be a difficult task, and the analysis was found be to very PSF dependent. Once the initial PSF has been obtained, it is then fitted, via cross-correlation, with the local maxima in the field to produce the relative astrometry and photometry in the field. The PSF is updated, subtracting companions from the stellar measurements, and the whole process can be restarted. A solution is typically found after a few iterations.

2.3. IDAC

IDAC is a publicly available cross-platform C++ code. The algorithm has also been described in detail elsewhere (Jefferies & Christou 1993; Christou et al. 1999). Basically, multiframe blind deconvolution assumes that a target field is observed multiple times with a different PSF for each observation. Using physical constraints for the imaging (e.g., finite pupil size, nonnegativity for the target and PSFs, and known noise statistics), estimates of the PSFs and target are convolved and compared with the observations. The difference is minimized iteratively using a conjugate-gradient technique. The multiple observations are important for obtaining a realistic solution, because the object is common and the PSF diversity drives the convergence. An error-metric minimization scheme drives the solution. The algorithm has been successfully applied to poorly compensated AO imaging of binary stars (Barnaby et al. 2000), and the data here represents a logical extension of its application. Initial estimates of the target and the PSF are needed for the MFBD algorithm. These are typically an averaged target image and a measured PSF through the optical system. The algorithm is then allowed to iterate. In practice, it has been found to be useful to hold the target solution fixed and to recompute the PSFs for a few iterations. The algorithm is then restarted, with both the target and PSF allowed to relax to a common solution. Both the target and PSF are solved for on a pixel-by-pixel basis, meaning that a large number of variables (i.e., image and PSF pixels) have to be minimized simultaneously. The photometry and astrometry of the reconstructed target was obtained using the IRAF APPHOT task. The densely crowded nature of this field made it very difficult to apply an aperture photometry algorithm to the data. Deconvolution reduces the spatial extent of each of the sources, reducing the PSF overlap so that aperture photometry can be applied.

2.3.1. Parametric Blind Deconvolution

This algorithm fits a parametric model to both the target and the PSF. The target model is the same as that for StarFinder, and the sensitivity of this technique rests on the PSF model chosen. Previous analysis has shown that low-order AO-corrected PSFs can be well modeled by an elliptical Lorentzian profile, and higher order AO-corrected PSFs by a combination of a co-located Lorentzian profile for the uncompensated wings and an Airy function for the diffraction-limited core (Drummond 1998; Barnaby et al. 2000). For these data, it was found that the Lorentzian-only profile provided the most consistent results. The fitting procedure starts off with a Lorentzian model for the brightest stars, and the residuals are used to update the number of stars. This iterative procedure is typically repeated several times.

3. ANALYSIS

3.1. Observed Data

3.1.1. StarFinder Analysis

All algorithms were applied to the four data frames shown in Figure 2. Figure 3 compares the object maps, using Gaussian

[3] See http://cfao.ucolick.org/software.

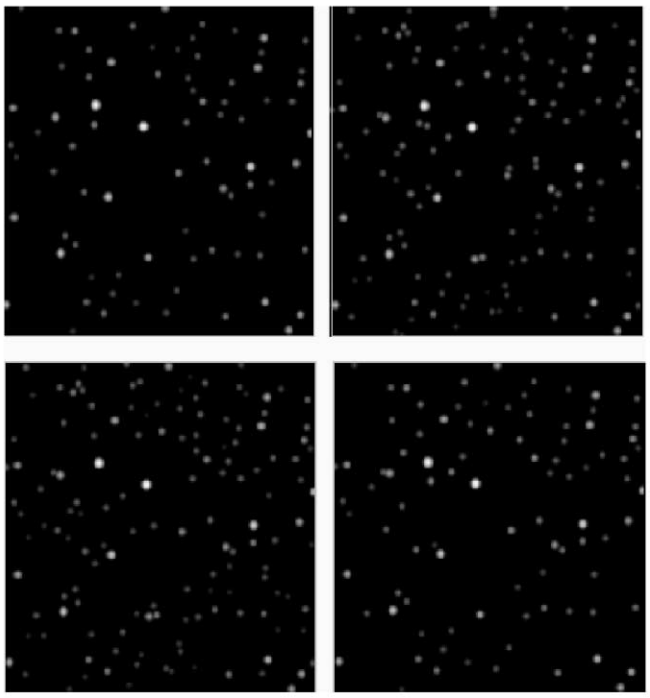

FIG. 3.—Reconstructed target maps for the StarFinder analysis of the four frames shown in Fig. 2. Note the difference in the number of identified stars for the different frames, and also how some of the closer stars in frames 2 (*top right*) and 3 (*bottom left*) are identified as single stars in the other two. There are 76 common stars between the four frames. All images displayed on a logarithmic scale.

PSFs, for the four separate frames from the StarFinder analysis. This illustrates how the quality of the compensation affects the number of stars identified. There were 79, 135, 142, and 91 stars for frames 1 to 4, respectively. Out of these, 76 stars were common to the four frames. For the poorer compensation cases (e.g., frames 1 and 4), it can be seen that close pairs of stars are not separable, and a single star is located that is not coincident with either of the two objects and so is not common. The common stars permit the measurement of the repeatability of the photometry and astrometry, thus giving an uncertainty for the measurements. These are shown in Figure 4 and indicate a trend, with a quadratic fit to the measurements, to larger errors at greater magnitude differences. For $\Delta m = 6$, the magnitude error is ~0.2 and the positional error is ~15 mas, which is less than a pixel and more than a factor of ~10 less than the FWHM of the stars in the raw data. These results indicate that under these poor conditions, reliable relative photometry can be estimated to within 0.1 mag.

3.1.2. IDAC Analysis

In contrast to the frame-by-frame analysis of StarFinder, the MFBD algorithm produces a single target reconstruction from the four frames. Figure 5 compares the common object map for the four Starfinder results shown in Figure 3 with the MFBD results and the common object PDB result discussed in the following section. It is important to also note that the reconstructed object uses no prior object information (i.e., a collection of point sources) and is computed on a pixel-by-pixel basis. Thus, extended non-pointlike structure can be seen in the reconstruction. This is especially true for the structure immediately below the brightest star in the field. Comparison with the second image from the StarFinder results in Figure 3 shows that this structure has been identified as two faint nearby sources. This represents one of the major differences between the two algorithms. StarFinder will search for pointlike structure only and can identify faint nebulous structure as a collection of point sources. By comparison, MFBD reconstructs the target as the best pixel-by-pixel fit with the data, and faint point sources may result in a faint extended structure.

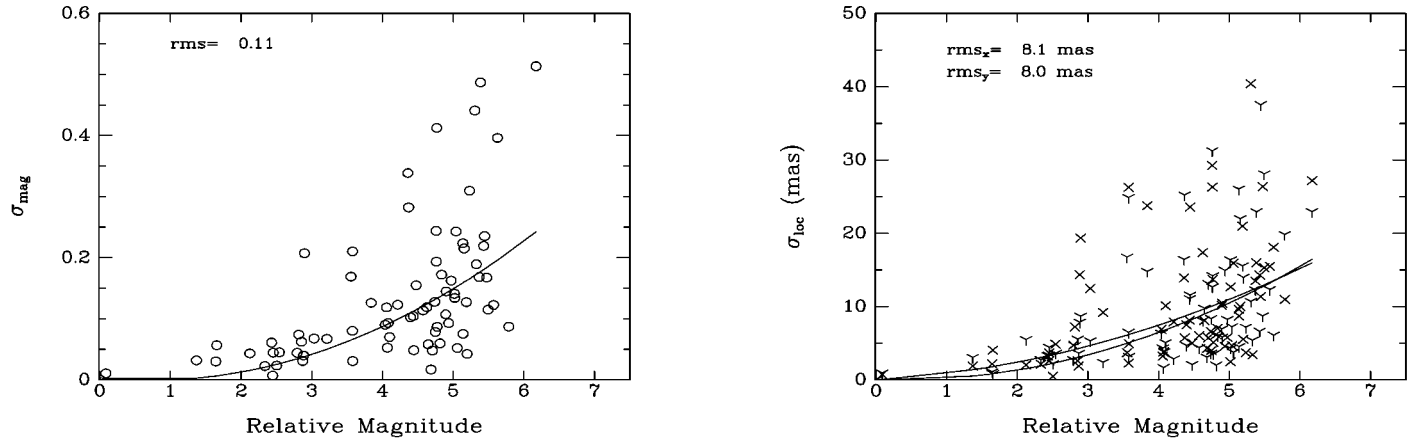

FIG. 4.—Measurements of the errors of the relative magnitudes and locations (illustrated by the *x* and *y* offsets, with the corresponding symbols) for the common stars from the StarFinder reductions shown in Fig. 3. Note the trend to larger errors for the fainter stars, illustrated by the quadratic fits to the data. In all of the plots, the magnitudes and magnitude differences are relative to the brightest sources in the field.

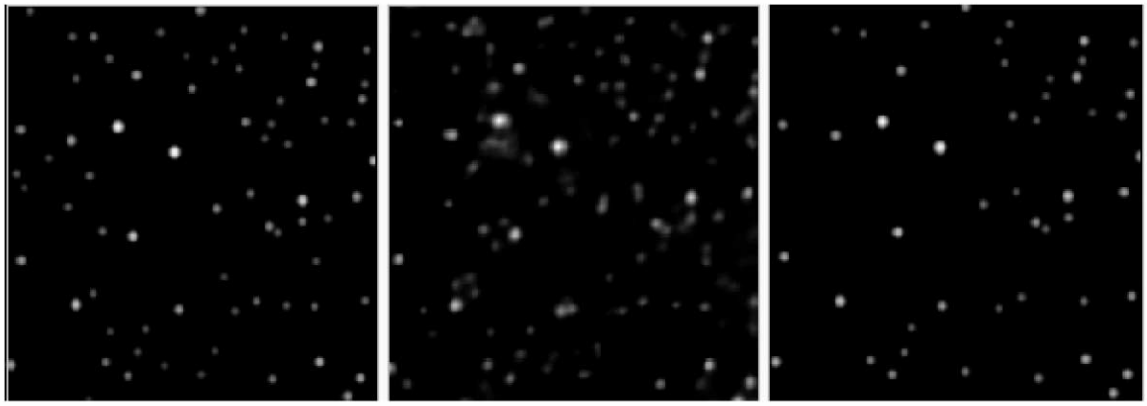

FIG. 5.—Comparison of reconstructed star maps: common stars for the four frames, using StarFinder (*left*), PBD (*right*), and the IDAC multiframe reconstruction (*center*). All images displayed on a logarithmic scale.

Photometry and astrometry of 119 targets in the deconvolved field were obtained using the IRAF aperture photometry task APPHOT. It has been noted that photometry on deconvolved images can overestimate the dynamic range within the data (in Hanisch & White 1993). Experience with the MFBD algorithm (Christou et al. 1999; Barnaby et al. 2000) has shown that peak photometry can suffer, but that the results are more accurate using aperture photometry. This is because in deconvolved images, fainter point sources can be restored with a larger spread than the brighter sources, because of signal-to-noise ratio (S/N) limitations. This data set contains many sources and therefore allows a more thorough investigation of the component widths, peak values, and relative brightness. This was investigated by comparing the aperture photometry with the width of the measured sources, and the results are shown in Figure 6. It can be seen that the fainter sources show a trend of an increase in size as the dynamic range in the image increases. This affects the relative magnitude, as determined from the peaks. It diverges from the relative magnitudes determined from the apertures and overestimates the magnitude difference by ~1 mag for $\Delta m \sim 8$. Given this analysis, we have used the aperture photometry to determine the relative brightness of the sources in the deconvolved field. We note that deconvolution minimizes the confusion between sources, permitting better aperture photometry to be done, but that some confusion will still remain for nearby sources in the field.

3.1.3. PBD Analysis

PBD was applied to the four frames independently. As for the StarFinder analysis, the number of stars identified depended on the frame. There were 78, 76, 78, and 63 stars located for the four frames, respectively, which was significantly fewer than the StarFinder analysis. The reconstructed star maps are

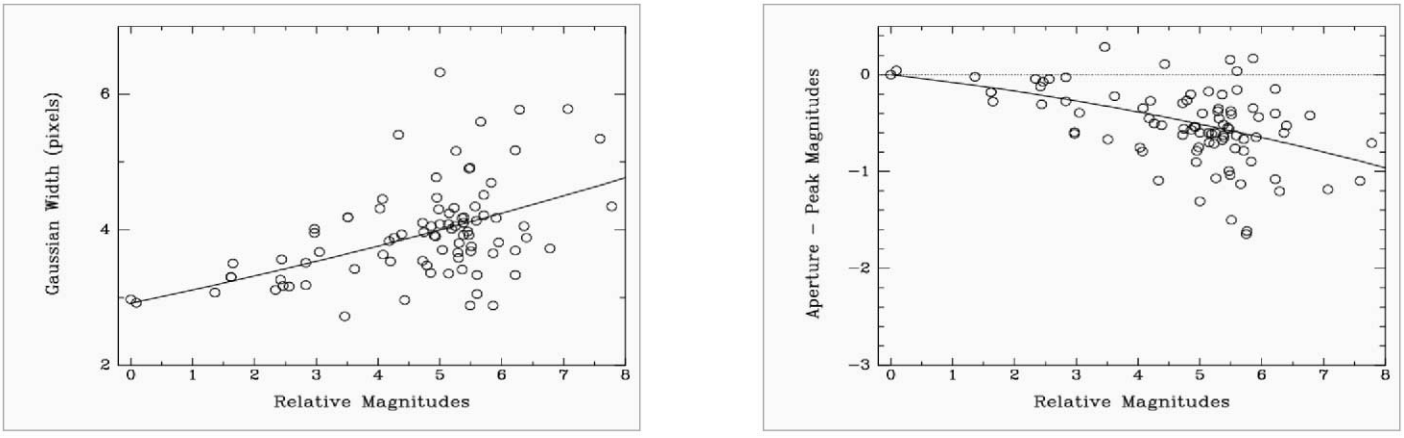

FIG. 6.—Photometry on the IDAC deconvolved image. *Left*: Gaussian width of the individual sources, compared to the aperture photometry relative to the brightest source. *Right*: Comparison of aperture and peak photometry from the MFBD results, showing the overestimation of the magnitude differences by using the peaks instead of the apertures. Quadratic fits to the distributions are shown, indicating the trends in the data.

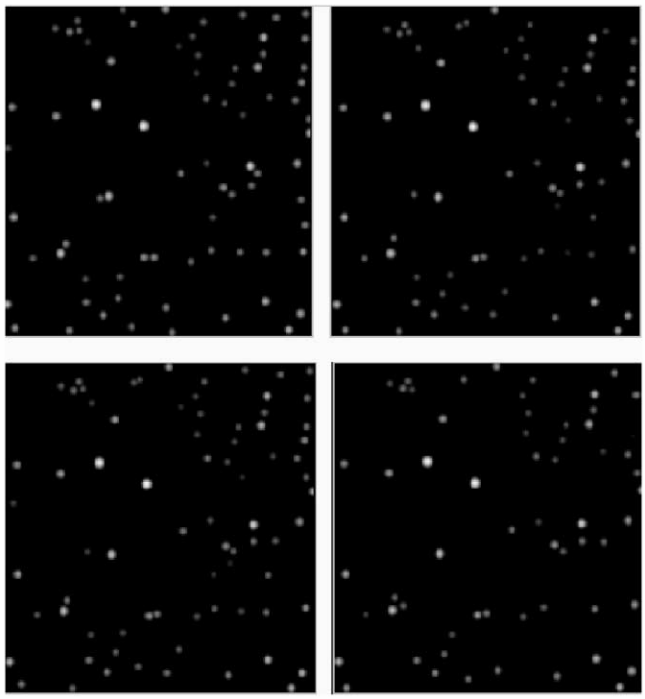

FIG. 7.—Reconstructed target maps for the PBD analysis of the four frames shown in Fig. 2. Note the difference in the number of identified stars for the different frames. Comparison with the StarFinder results in Fig. 3 shows fewer identified stars, especially the fainter sources near the two brightest. There are 57 common stars found in the four frames. Images displayed on a logarithmic scale.

shown in Figure 7. Comparison with the four-frame StarFinder results in Figure 3 shows that this algorithm fails to identify the fainter stars hidden in the extended halos of the brightest two stars in the field. The 57 common stars in the four frames have an rms dispersion of 0.19 mag, compared to the 0.12 mag for the same stars from the StarFinder analysis. The astrometric dispersion is ~10 mas, which is comparable to the StarFinder analysis. A detailed analysis of the dispersions show that both magnitude and position are more poorly determined for the fainter sources, as shown in Figure 8, similar to the StarFinder analysis. The PBD analysis truncated the measured magnitude range to ~5.5, less than the other two techniques.

3.1.4. Comparison of Techniques

The previous section has shown how the photometry and astrometry can be obtained from the observed data using two direct model fitting techniques, StarFinder and PBD. Figure 9 compares the relative photometry and astrometry for the StarFinder and IDAC using the 68 stars that are common to the three images in Figure 5. The brightest star in the field is used as the reference for both brightness and position. The astrometry is in very good agreement, with an rms offset between the two techniques of ~1 pixel (19 mas), and lower for stars within 4 mag of the reference. The photometry is also in good agreement for a dynamic range of under 4 mag, but shows a trend such that fainter stars in the field are relatively brighter for the StarFinder analysis compared to the aperture photometry on the IDAC image. This trend suggests that the StarFinder magnitudes are ~0.5 brighter than the MFBD results for a dynamic range of 6 mag. Figure 10 shows the same comparison for the StarFinder and PBD results, indicating an opposite trend in the magnitude differences.

3.1.5. Point-Spread Function Reconstructions

All three algorithms solve for the PSF. Both StarFinder and IDAC solve for a numerical PSF on a pixel-by-pixel basis, whereas PBD obtains a model fit, in this case an elliptical Lorentzian profile. The quality of the reconstructed PSFs can be compared and are shown in Figure 11. The cores of the numerical PSFs show very similar structure, with the major differences being in the wings. For the MFBD analysis, the PSF is reconstructed over the whole field. However, for the StarFinder analysis, there was a trial-and-error learning curve to determine which size PSF window to use, because of the crowded nature of the field. Eventually, it was determined that a 90 × 90 pixel size (1.″7 × 1.″7; the field shown in Fig. 11), was optimal. However, a circular cut-off at a radius of 40 pixels (750 mas) had to be used to limit nearby source contamination, thus artificially limiting the extent of the PSF. By comparison, no cut-off was used for the MFBD analysis, allowing the PSF to extend further. These low-level PSF wings would reduce the strength, and also affect the locations, of fainter sources in the field when compared with the truncated PSFs used for the StarFinder analysis. The PBD PSFs show a strong similarity to the numerical PSFs; the cores match well and the wings appear to be stronger. Because of the inherent symmetry in the model, the PBD process is not able to replicate more complex structure, such as the flaring in the core for the first frame of the two numerical results. The azimuthally averaged radial profiles for the first frame PSF for the three methods are shown in Figure 12. The profiles of the PSF cores match well to ~0.″3, and then the analytic model of the PBD result causes divergence, indicating that the model has too few parameters. The StarFinder and IDAC profiles match very well out to the wings of the PSF at ~0.″55, where the StarFinder profiles shows the artificial roll-off due to the limited size PSF extraction window discussed earlier.

3.2. Simulations

The above analysis shows that the three techniques yield similar photometry and astrometry for relatively small magnitude differences, but significant differences for larger magnitude differences. The number of stars found depends upon both the data quality and the algorithm.

The accuracy of the StarFinder and IDAC techniques was investigated by simulating this same field based on the recon-

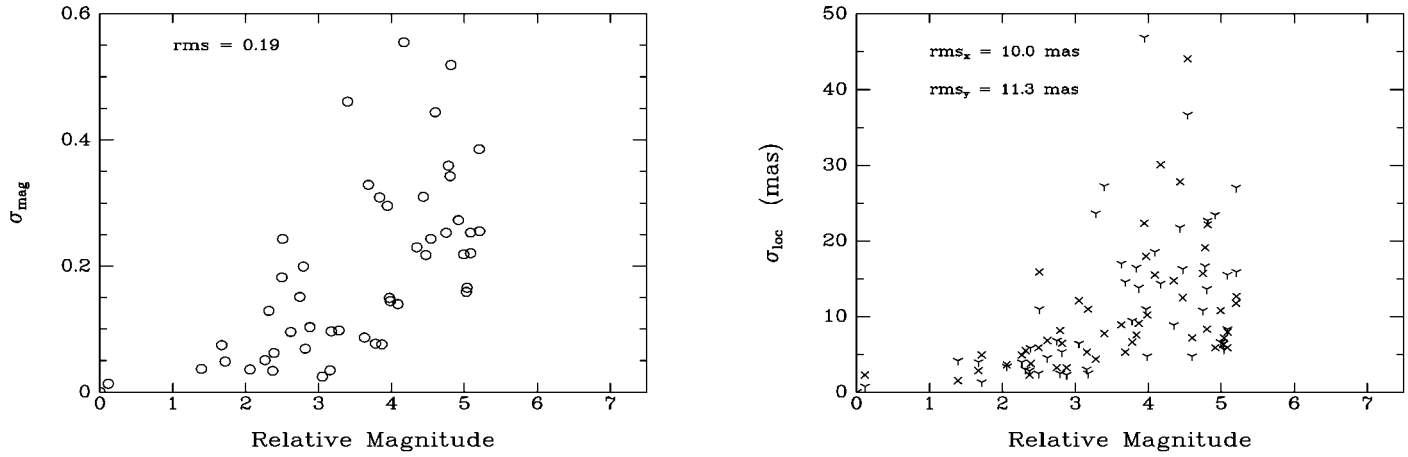

FIG. 8.—Measurements of the errors of the relative magnitudes and locations (illustrated by the *x* and *y* offsets, with the corresponding symbols) for the common stars from the PBD reductions shown in Fig. 7. Note the trend to larger errors for the fainter stars, similar to that for the StarFinder results. In all of the plots, the magnitudes and magnitude differences are relative to the brightest sources in the field.

structed StarFinder PSFs and the locations and relative brightnesses of the 142 stars obtained from the StarFinder analysis of the third image of the four-frame subset. Read noise similar to that measured for the observations was then added, and the four synthetic images are shown in Figure 13.

These simulated data were analyzed in the same way as the observations. StarFinder was applied to each of the frames individually, and IDAC was applied to the four simultaneously, in both cases assuming that the PSFs were unknown. Figure 14 compares the true map with the map of common stars from the four StarFinder results and the IDAC object reconstruction. The true and StarFinder images were generated from the respective maps with Gaussian PSFs equivalent to those in the IDAC reconstruction. Visual comparison of the IDAC reconstruction shows most of the stars from the true image, but there are also artifacts near the brighter stars that are not present in the true image. These artifacts appear as faint streaks below the two brightest stars in the field, and as such are not identified as extra point sources. They are due to the nature of the simulations, in that the StarFinder-produced PSFs have hard edges at a radius of 40 pixels that were not completely smoothed out before convolving with the object (see Fig. 12).

As for the observed data, the photometry and astrometry for the IDAC result was obtained using the IRAF APPHOT aperture photometry package. This was also applied to the true field in order to determine the precision of the package when applied to such a field distribution. The relative photometry of the true image was recovered to within an rms error of 0.04 mag evenly distributed over the 7 mag dynamic range of the simulations, and the relative astrometry was recovered with

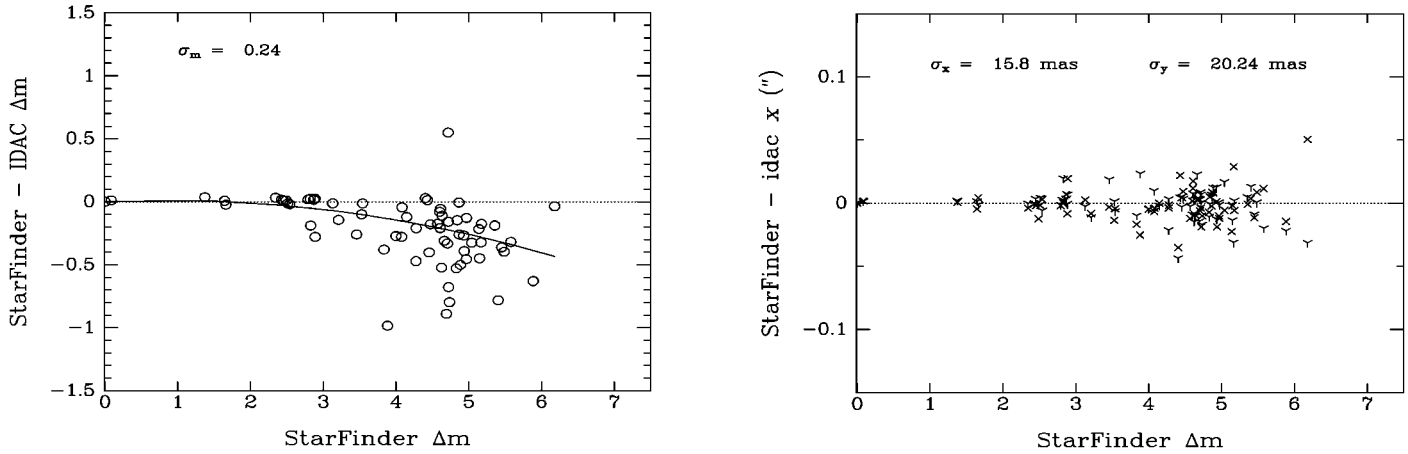

FIG. 9.—Comparison of the relative photometry (*left*) and astrometry (*right*) from StarFinder and MFBD. The aperture photometry from the IDAC results underestimate the brightness of the fainter sources in the field by ~0.5 mag. The relative astrometry is in good agreement to within ~1 pixel.

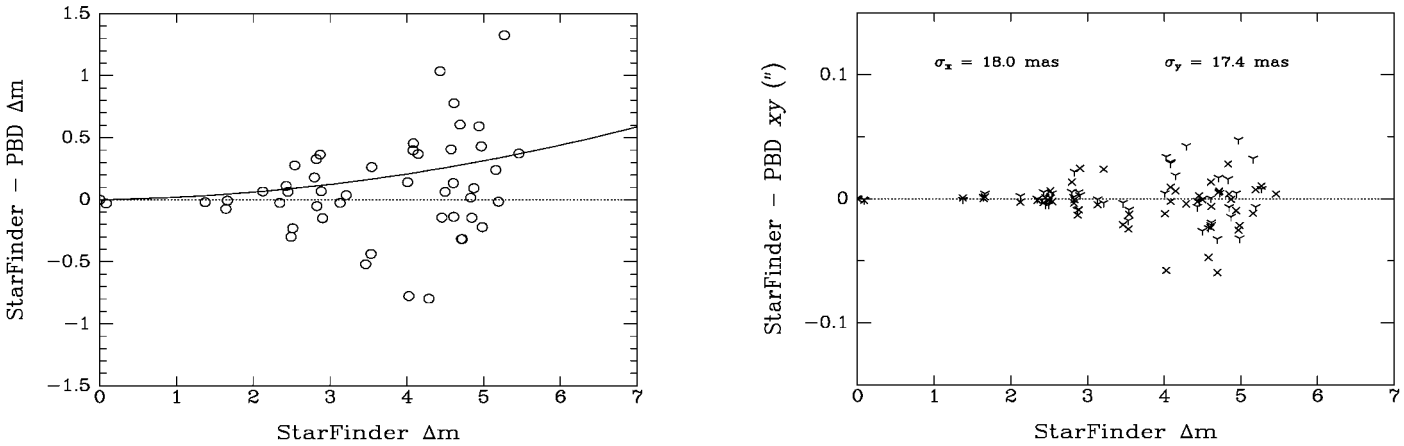

FIG. 10.—Comparison of the relative photometry (*left*) and astrometry (*right*) from the two model fitting approaches, StarFinder and PBD. The PBD photometry overestimates the brightness of the fainter sources in the field by ~0.5 mag, compared to the StarFinder results. The relative astrometry is in good agreement, to within ~1 pixel.

an rms error of 1.5 mas similarly evenly distributed over the dynamic range. These measurements indicate that the APPHOT package is suitable for the type of data shown in the IDAC reconstructions.

Figure 15 examines the relative photometry for StarFinder and IDAC, comparing the results with the true field and with each other. As for the observed data, the brightest source was used as the reference. The stars were identified by matching their locations to the true positions to within a radius of 3 pixels. The IDAC image yielded 85 stars measurable by APPHOT, whereas the combined StarFinder result yielded 63 stars. Of these, only 59 were in common with the IDAC result. Apart from the artifacts described above, the IDAC images did not create any false targets. These artifacts were inherent in the synthetic data to begin with. On the other hand, the combined StarFinder result misidentified four stars because of blending effects that identified a close pair as a single object, as can be seen by comparing the images in Figure 14.

The StarFinder photometry shows very good agreement of the common stars with the true field. The rms error is 0.10 mag, with a very good agreement down to a 4 mag dynamic range, and with larger errors below that. By comparison, the IDAC photometry has a larger rms error of 0.25 mag. However, as with the StarFinder results, the significant errors occur for dynamic ranges above 4 mag. Both results do not show any major systematic trends and are relatively evenly distributed about the

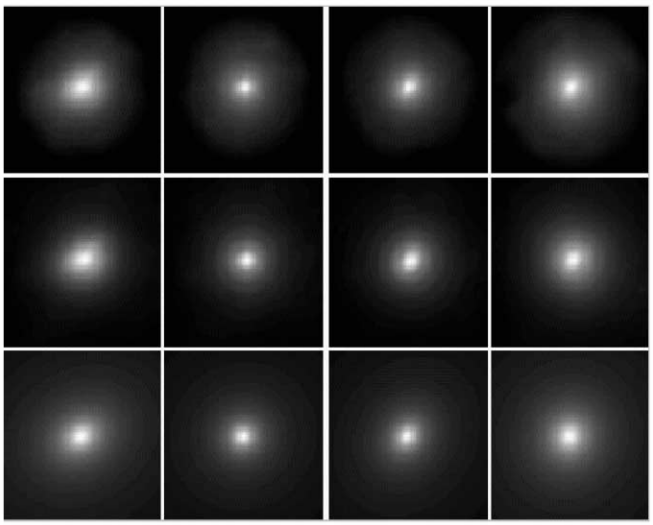

FIG. 11.—Reconstructed PSFs for frames 1–4 (*left to right)* from StarFinder (*top)*, IDAC (*center*), and PBD (*bottom*). All images displayed on a square-root scale.

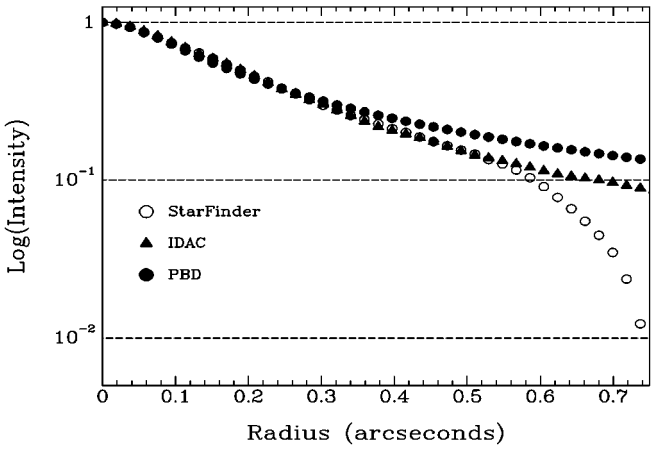

FIG. 12.—Azimuthally averaged radial profiles of the reconstructed PSFs for frame 1 for the three algorithms. The StarFinder and IDAC profiles match very well up to the intensity fall-off due to the StarFinder PSF extraction box used (40 pixels). The analytical PBD PSF matches out to ~0.″3 and then significantly diverges from the other two.

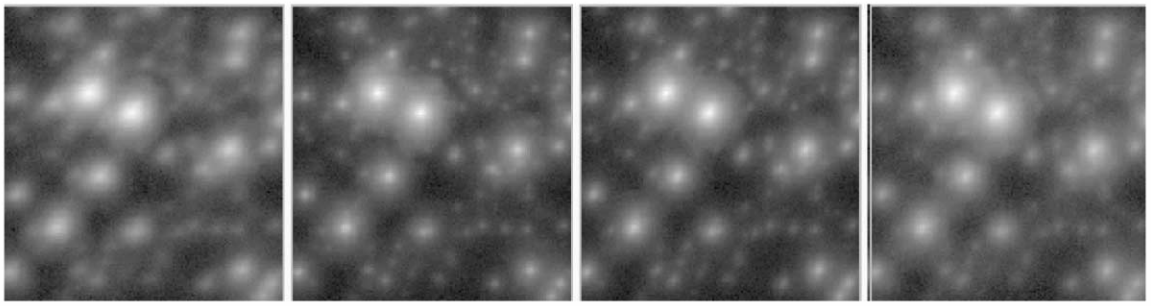

FIG. 13.—Simulated fields representing the four observed subfields (*left to right*). These were generated using the StarFinder target map for the third subfield and the reconstructed PSFs for the four observations from the StarFinder analysis. All images displayed on a logarithmic scale.

zero-error line. The IDAC result shows some stars to have errors over 0.5 mag, especially at high dynamic range, and there are also a couple of outliers that are the result of contamination from nearby sources in the aperture photometry.

Comparing the results between the two reductions for the common stars, we see no systematic trend, as we did for the observed data. The rms difference between the two results is 0.18 mag, with good agreement down to a 4 mag dynamic range, less than for the observed data. The outlier, once again, is due to contamination in the IDAC photometry. The relative astrometry from both analyses is equivalent, with rms errors of approximately 10 mas, which is better than the observed data, and with no systematic trends. The lack of a systematic trend between the two techniques is not surprising, given that the StarFinder PSF, with its restricted extent, was used to generate the simulated data. This supports the conjecture that the extended wing structure in the actual PSFs affects the quantitative measurements.

4. DISCUSSION

Measurements of photometry and astrometry for AO-corrected images rely upon some knowledge of the PSF of the observations. AO PSFs are not always well behaved and can have a complex structure, due to the nature of the compensation. A number of algorithms have been developed to measure the photometry and astrometry and to reconstruct the PSF at the same time. We have compared three of these techniques, all of which are variants of a blind deconvolution analysis, ranging from full pixel-by-pixel reconstruction to parametric analysis of both the point-source field and the PSF. The test data was a segment of a crowded field from Gemini/Hokupa'a Galactic center *K*-band imaging for which the PSFs from the individual stars overlapped significantly with low-order adaptive optics compensation.[4] The algorithms used were StarFinder, a pixel-by-pixel PSF-fitting algorithm that directly measures the position and intensity of the sources; IDAC, an iterative pixel-by-pixel multiframe blind deconvolution code; and a parametric blind deconvolution code that measures the position and intensity of the point sources by fitting a model PSF.

It was found that both StarFinder and the PBD algorithms were sensitive to the S/N of the data for detection of the faint sources, with more targets being found for the higher Strehl

[4] See http://www.us-gemini.noao.edu/gallery/science/gal_center.html.

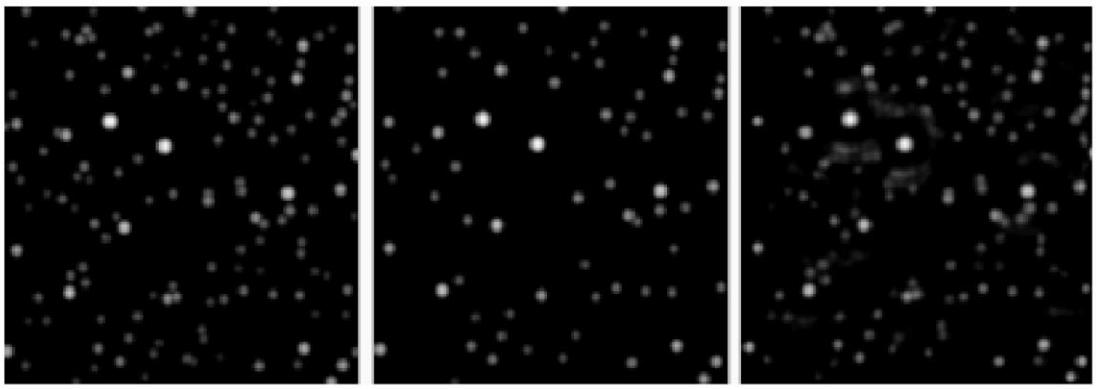

FIG. 14.—True field (*left*) compared with the common stars for the StarFinder (*center*) and IDAC results (*right*). There are fewer stars in the StarFinder result, because the analysis is both S/N and PSF dependent. Fewer stars were identified in the poorer compensated frames. Note that the IDAC reconstruction shows most of the stars in the true image, but there are also some artifacts, which are clearly visible nearer the brighter stars. All images displayed on a logarithmic scale.

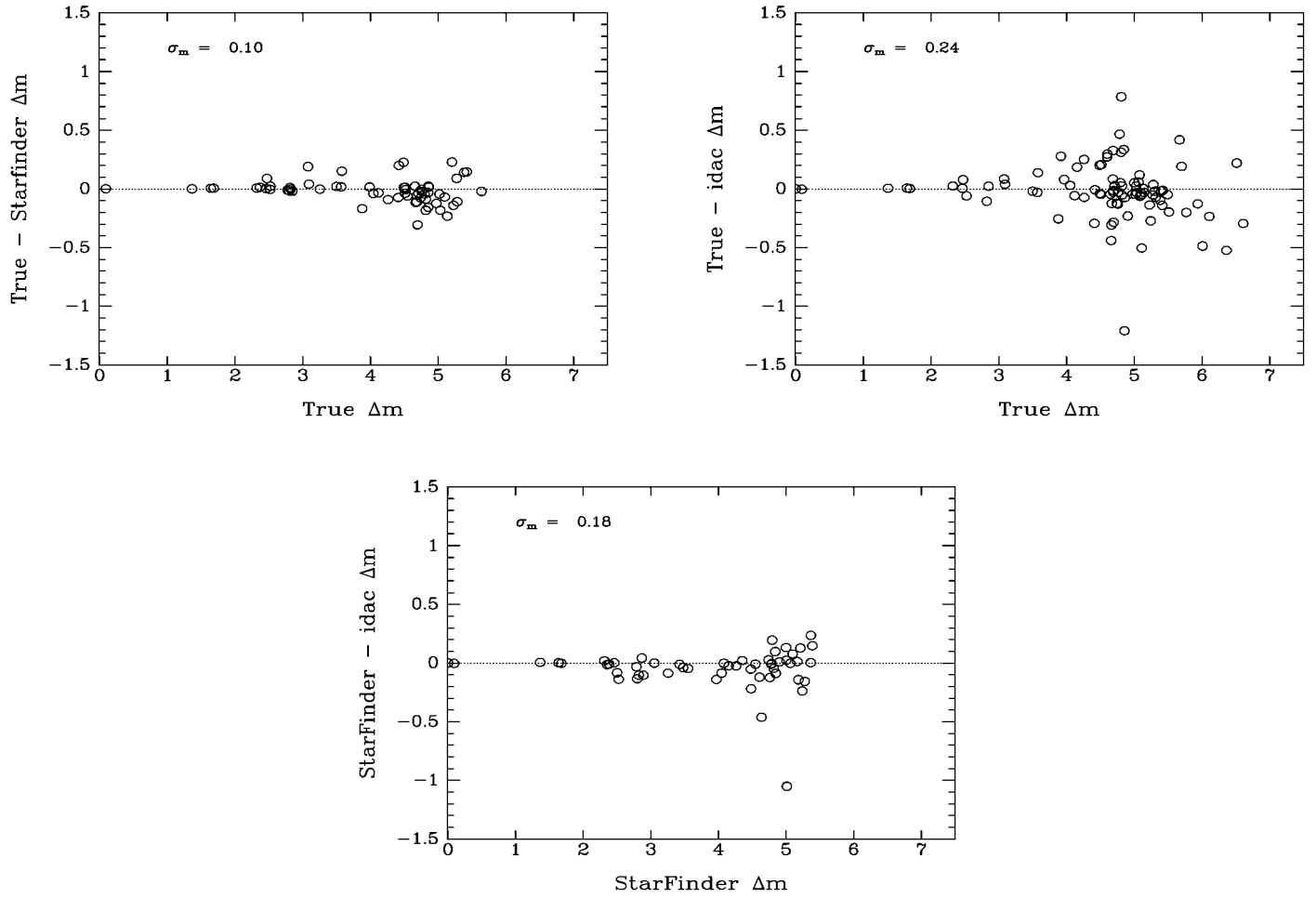

FIG. 15.—Comparison of the relative photometry from the common StarFinder stars (*top left*) and the IDAC stars (*top right*) with the true field for the simulated data set. The bottom plot shows the comparison of the StarFinder and IDAC results.

ratio images. IDAC, the multiframe blind deconvolution algorithm, was applied to all four measurements simultaneously. The analysis presented here shows that the three algorithms are capable of recovering self-consistent photometric and astrometric results from these data for dynamic ranges of below 4 mag. At larger mag differences, the astrometry is consistent to within 20 mas, compared to a diffraction limit of 58 mas and a PSF size of 200 mas, but the photometry diverges. Using the StarFinder results as the reference, the IDAC photometry underestimates the relative magnitudes by up to 0.5 mag for dynamic ranges of 6 mag, and the PBD results overestimate by the same amount. The astrometric differences between the analyses from the three techniques are relatively small, although the rms difference is greater than the scatter of the measurements from the four different StarFinder reductions. The difference is still a factor of 10 less than the FWHM of the stars in the raw AO data.

Comparison of the StarFinder and IDAC algorithms to data simulating these observations show a photometric agreement between the two to be about 0.18 mag, but with a greater dispersion for the IDAC results at greater magnitude differences when compared with the true values. The IDAC deconvolved images showed a trend of increasing target width with increasing dynamic range, so that peak-value fitting would yield incorrect photometry, thus yielding a greater dynamic range in target brightnesses within the image. The results here confirm that aperture photometry on the deconvolved images is essential, yielding values that are similar to that of PSF fitting and are in good agreement with the true values for the simulated data. We note that the StarFinder analysis is sensitive to the PSF, identifying a different number of targets as the PSF structure changes. For the synthetic data, approximately 50% of the stars were identified from the combined results for the four frames. However, the best frame identified ~90 stars by blending two stars with close separation into a single target. The synthetic data showed that this happened at least four times. The IDAC image of the synthetic field recovered most of the stars (~90%), but not all were

readily measurable by APPHOT. It could be that a more sophisticated algorithm such as ALLSTARS may have worked better.

The reconstructed PSFs from these three algorithms are very similar in their cores, with the major differences occurring in the wings; this accounts for the greater differences in photometry between the algorithms. The parameterized PSF of PBD is limited, in that it cannot take into account nonsymmetric structure in the PSFs.

The observations used here represent poor AO performance, with Strehl ratios less than 5% that are not typical for current AO systems. It is expected that the performance of these algorithms should improve with significantly better data. However, one drawback is the anisoplanatic nature of current AO systems for wide fields, which will become more significant as the Strehl ratios improve.

This work has been supported by the National Science Foundation Science and Technology Center for Adaptive Optics, which is managed by the University of California at Santa Cruz under cooperative agreement AST 98-76783. We would like to thank the Gemini team for making these data publicly available, Sasha Hinkley and Soeren Larsen for their assistance, and Laird Close for very constructive feedback.

REFERENCES

Barnaby, D., Spillar, E., Christou, J. C., & Drummond, J. D. 2000, AJ, 119, 378
Christou, J. C., Bonnacini, D., Ageorges, N., & Marchis, F. 1999, ESO Messenger, 97, 14
Diolaiti, E., Bendinelli, O., Bonaccini, D., Close, L., Currie, D., & Parmeggiani, G. 2000, A&AS, 147, 335
Drummond, J. D. 1998, Proc. SPIE, 3353, 1030
Flicker, R. C., & Rigaut, F. J. 2002, PASP, 114, 1006
Fusco, T., Véran, J.-P., Conan, J.-M., & Mugnier, L. M. 1999, A&AS, 134, 193
Graves, J. E., Northcott, M. J., Roddier, F. J., Roddier, C. A., Potter, D., O'Connor, D. J., Rigaut, F. J., & Chun, M. R. 2000, Proc. SPIE, 4007, 26
Hanisch, R. J., & White, R. L. 1993, Proc. STScI Workshop, the Restoration of *HST* Images and Spectra II, ed. R. J. Hanisch & R. L. White (Baltimore: STScI)
Jefferies, S. M., & Christou, J. C. 1993, ApJ, 415, 862
Roth, K. C., Guyon, O., Chun, M., Jensen, J. B., Jorgensen, I., Rigaut, F. J., & Walther, D. M. 2001, BAAS, 33, 785